Robust graphene-based molecular devices

Maria El Abbassi,[†,‡,¶] Sara Sangtarash,[§] Xunshan Liu,[‖] Mickael Perrin,[†] Hatef Sadeghi,[*,§] Oliver Braun,[†,‡] Herre S.J. van der Zant,[¶] Shlomo Yitzchaik,[⊥] Silvio Decurtins,[‖] Shi-Xia Liu,[*,‖] Colin Lambert,[§] and Michel Calame[*,†,‡,#]

†*Empa, Swiss Federal Laboratories for Materials Science and Technology, Transport at nanoscale interfaces Laboratory, CH-8600 Dübendorf, Switzerland.*

‡*Department of Physics, University of Basel, Klingelbergstrasse 82, CH-4056 Basel, Switzerland*

¶*Kavli Institute of Nanoscience, Delft University of Technology, Lorentzweg 1, 2628 CJ Delft, The Netherlands*

§*Quantum Technology Centre, Department of Physics, Lancaster University, Lancaster LA1 4YB, United Kingdom*

‖*Department of Chemistry and Biochemistry, University of Bern, 3012 Bern, Switzerland*

⊥*Institute of Chemistry, The Hebrew University of Jerusalem, Jerusalem, 91904, Israel*

#*Swiss Nanoscience Institute, University of Basel, 4056 Basel, Switzerland.*

E-mail: h.sadeghi@lancaster.ac.uk; shi-xia.liu@dcb.unibe.ch; michel.calame@empa.ch

Abstract

Understanding charge transport at the level of a single to a few molecules is of great importance for both fundamental research and applications in electronic devices. To upscale the production of molecular devices, one of the main challenges is to contact molecules in a controlled and reliable way. In this study, we report on the realization of a mechanically and electronically robust graphene-based molecular junction. This is achieved by separating the requirements for both types of stability at the molecular level. The mechanical stability is obtained by anchoring molecules directly to the substrate using silanization, rather than to graphene electrodes. The electronic stability is achieved by adjusting the π-orbitals overlap of the conjugated head groups between neighbouring molecules. The molecular devices exhibit stable current-voltage (IV) characteristics up to bias voltages of 2.0 V with reproducible transport features in the temperature range from 20 K to 300 K. By providing stable and reproducible nanometer-scale devices preserving coherent transport properties up to room temperature, our approach represents a unique opportunity for the future development of molecular-scale devices.

Introduction

Layered materials have found a wide range of applications,[1] ranging from high power battery cells[2] to (bio-)sensors[3–5] and optoelectronics circuit components.[1,6] In particular for electronic and optoelectronic purposes they have generated considerable interest, being used as building block for transistors,[7] photodetectors,[8] artificial neurons[9] and memristors for non-volatile random-access memory and neuromorphic computing.[10–12] Due to its unique mechanical,[13] optical[14] and electronic[15] properties, graphene is, in this context, an appealing electrode material for planar molecular devices.[16–19]

To upscale the fabrication of molecular devices, one of the main challenges is to achieve a mechanically stable device with reproducible and controllable electronic features, oper-

ating at room temperature.[20,21] This is crucial, as structural and electronic fluctuations in the system can lead to significant changes in the transport characteristics of the graphene-molecule interfaces.[22,23] To realize reliable graphene-based junctions, several issues exist to date and need to be addressed. First, graphene-based junctions have been reported to exhibit signatures similar to those of molecules, with gate-dependent resonance features, such as Coulomb blockade,[24,25] quantum interference[17] and Fabry-Perrot resonances.[26] Second, connecting molecules to the graphene remains challenging due to the lack of control on the electrode geometry at the nanoscale.[16,19,23,24,26] Moreover, achieving both mechanical stability and electrical reproducibility at the same time impose different requirements on the junction properties.[22,27] Finding the proper balance between electronic and mechanical stability is challenging. Weakly coupled $\pi - \pi$ stacking is believed to be an appealing strategy to anchor the molecules to the electrodes,[22] offering advantages such as high thermoelectric efficiency. However, this approach has been shown to lead to mechanically unstable junctions.[28] Alternatively, molecules have also been bonded covalently to graphene, yielding mechanically stable junctions.[19] However, transport through strongly coupled molecules is expected to be heavily influenced by the electrode geometry, edge termination and crystallographic structure, leading to a large variability in the shape of the current-voltage characteristics.[22] Third, junction-to-junction variability remains high for the above-mentioned anchoring methods,[29,30] leading to poor devices reproducibility. Finally, the silicon dioxide substrate itself has been reported to yield feature-rich charge-transport characteristics,[31] in particular due to switching within the oxide,[32] which may be confused with molecular signatures.

Junction geometry

In this study, we propose a new strategy to achieve stable and reproducible graphene-based molecular junctions by separating the strong mechanical anchoring from the electronic path-

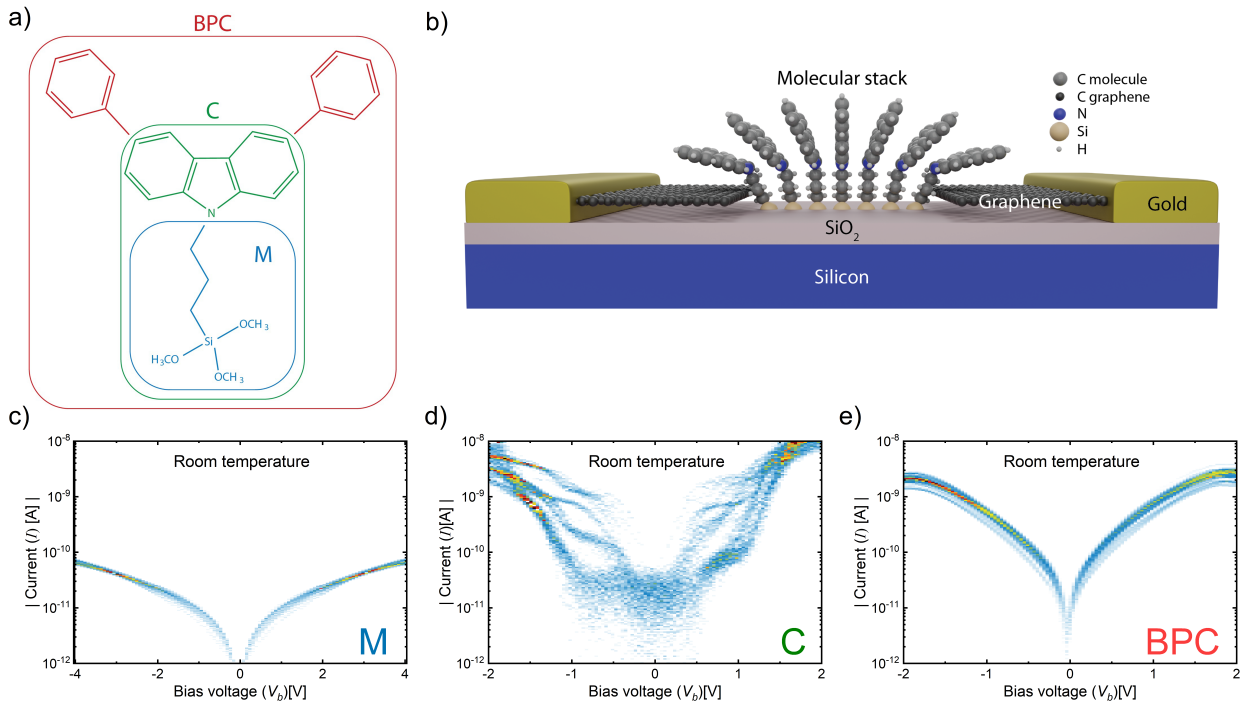

Figure 1: **Junction Geometry and molecular design** a) Drawing of the three molecules, constituted of three main parts: the silane group for the covalent anchoring to the substrate, the alkane chain that decouples the silane group from the head group : CH_3 (molecule M) , N-carbazole (molecule C), and bi-phenyl N-carbazole (molecule BPC). b) Schematic illustration of a molecular junction containing a series of π-π-stacked molecules bridging a graphene nanogap. The atomic positions of the molecules are for illustrative purposes only, and do not correspond to the DFT-relaxed geometry shown in Figure 4. The nanogaps are formed using the electrical breakdown technique.[33] The molecules are attached to the substrate via silanization of the surface. For clarity reasons the scales are not accurate and different colours are used to distinguish carbon atoms of the molecule from those of the graphene. c-e) The electrical measurements corresponding to the three molecules under study with different head groups are displayed as density plots of the measured IVs, of which the absolute value of the current is plotted on logarithmic scale. For each molecule, 100 IVs without data selection are measured at room temperature on a specific device per molecule.

ways. Our approach allows for coherent transport through the molecular devices, resulting in a low temperature dependence. This was realized by combining the high structural stability of graphene electrodes (even at room temperature[16]) with a specifically designed molecule, shown in Fig. 1a. The molecule contains three main parts, a silane group and a π-conjugated head group, decoupled by a non-conjugated alkane chain. The silane part is responsible for the mechanical anchoring of the molecule by forming a covalent bond with the substrate. This

silanization process is commonly used to cover surfaces with organofunctional molecules.[34–36] This approach offers distinct advantages. As the graphene edges usually present ill-defined edge terminations after nanofabrication and/or preparation of the contact electrodes, anchoring the molecules to the substrate seems a valid possible alternative. Moreover, as the molecules are covalently bound to the substrate, this process leads to mechanically stable graphene-molecule junctions. Finally, the silanization process also passivates the silicon dioxide surface and prevents unwanted switching effects.[32] The second part of the molecule is the conjugated head group, specifically a bi-phenyl N-carbazole group (molecule BPC), whose orbitals can couple to the π orbitals of the graphene. The alkane chain is the final necessary element, whose crucial role is to electronically decouple the mechanical anchoring from the electronic head group. DFT calculations (see Supplementary Information) confirm that the frontier orbitals of the BPC molecule are indeed solely located on the head group. These calculations also show that head groups of two neighbouring molecules can $\pi - \pi$ stack, forming transport channels which are delocalized across all head groups. A schematic illustration of BPC molecules assembled in the graphene nanogap with $\pi - \pi$ stacked head groups is shown in Fig. 1b).

In order to correlate the junction stability and electrical properties with the molecular structure, several test molecules with different head groups were designed and investigated. The first test molecule is methyl terminated (in the following abbreviated as molecule M). Due to the absence of a delocalized π system, it is expected to only poorly conduct charges. The second test molecule possess an N-carbazole head group (in the following abbreviated as molecule C). The π-system of molecule C has two phenyl rings less than the BPC molecule. The lack of phenyl rings leads to a reduction in orbital overlap by about a factor of 2, resulting in a lower interaction energy between neighboring head groups.[22] Due to its smaller interaction energy, molecule C is therefore expected to form less stable transport channels than the BPC molecule.[22]

The molecular junctions were formed as follows. First, nanogaps were created in the

graphene devices using the electrical breakdown technique, as described in previous studies.[16,18,33] The graphene gaps were first characterized at room- and low temperature, before deposition of the molecules. Only junctions with resistances higher than 1GΩ and showing no gate dependence were selected for further use. After characterization of the empty gaps, the devices were immersed for 20 hours at 80 degrees in a solution containing dry toluene and the molecules of interest (0.1 mM). The samples were then successively rinsed with dichloromethane, acetone and isopropanol.

Figure 1c)-e) presents the electrical characterisation of three devices, each exposed to one of the molecules under study. For this purpose, current-voltage characteristics (IVs) are acquired at room temperature by averaging a back-and-forth voltage sweep. For each device, 100 IVs are measured and combined into a density plot without any data selection. This density plot consists of a 2-dimensional histogram of all IVs recorded on the device, constructed by binning both the current and the voltage axes. For the current axis, the absolute value of the current on log-scale is used. The density plots are a color-coded representation of such histograms, in which areas of high counts can be identified, corresponding to the most likely device behaviour. The density plots are normalized by the total number of data points.

The junction containing molecule M (Fig. 1c) presents a single category of tunnelling-like IV curves, with a maximum current of about 10 pA at a bias voltage of 2 V. The IVs recorded on junctions exposed to molecule C are shown in Fig. 1d. The maximum currents are about two orders of magnitude larger than for molecule M, indicating that the π-π stacking allows for more efficient charge transport across the molecular junction. However, the plot also exhibits large variations in IV shapes and current levels. These fluctuations are attributed to the weak electronic interaction between the neighbouring head groups, allowing for various molecular conformations to occur, each of them possibly with slightly different electronic properties. Figure 1e shows the density plot of the IV curves recorded for a device after deposition of molecule BPC. Contrary to molecule C, the BPC molecule leads to both

a higher current and a higher stability, as shown by the high similarity of the 100 IV curves recorded at room temperature.

Stability and intersample reproducibility at 20 K

To achieve a more in-depth spectroscopic characterization of the BPC molecular junctions, electrical measurements were performed at cryogenic temperatures (20 K). Figure 2 presents an overview of these measurements, with Fig. 2a showing three individual IV-curves recorded on each device. 100 of such IVs are measured successively, and plotted as an evolution plot (Fig. 2b). Here, the amplitude of the current is color-coded and plotted versus bias voltage and IV number. The plots show that the devices are stable over time, with only minor fluctuations observed. Furthermore, all devices exhibit similar current levels (within one order of magnitude) and curve shape. The 100 IVs are then used to construct a density plot (Fig. 2c), as described previously. Here, only one category of IVs is observed, with small fluctuations. The inset shows the corresponding average IV ($\langle I \rangle$), exhibiting a very similar shape as the individual IVs shown in Fig. 2a. Finally, the numerical derivative of $\langle I \rangle$ is calculated (Fig. 2d) in order to obtain the differential conductance ($\mathrm{d}\langle I \rangle/\mathrm{dV}$) traces (blue line). As a comparison, the red traces display the dI/dV curve for that particular device obtained at 20 K before deposition. The observed resonance peaks are a signature of one or more transport channels present in the molecular junction. As these resonances are only present after deposition of molecules, they are attributed to the presence of the BPC molecule. In general, the position of these resonances reflects the electronic structure of the junction. These resonances are located at similar bias voltages, highlighted by the grey-shaded regions, confirming the robustness and reproducibility of the BPC molecular junctions. We note, however, that the resonances exhibit different amplitudes, which may be attributed to local variations in the junction conformation.

Finally, we note that also for molecule C, the mechanical anchoring to the substrate is

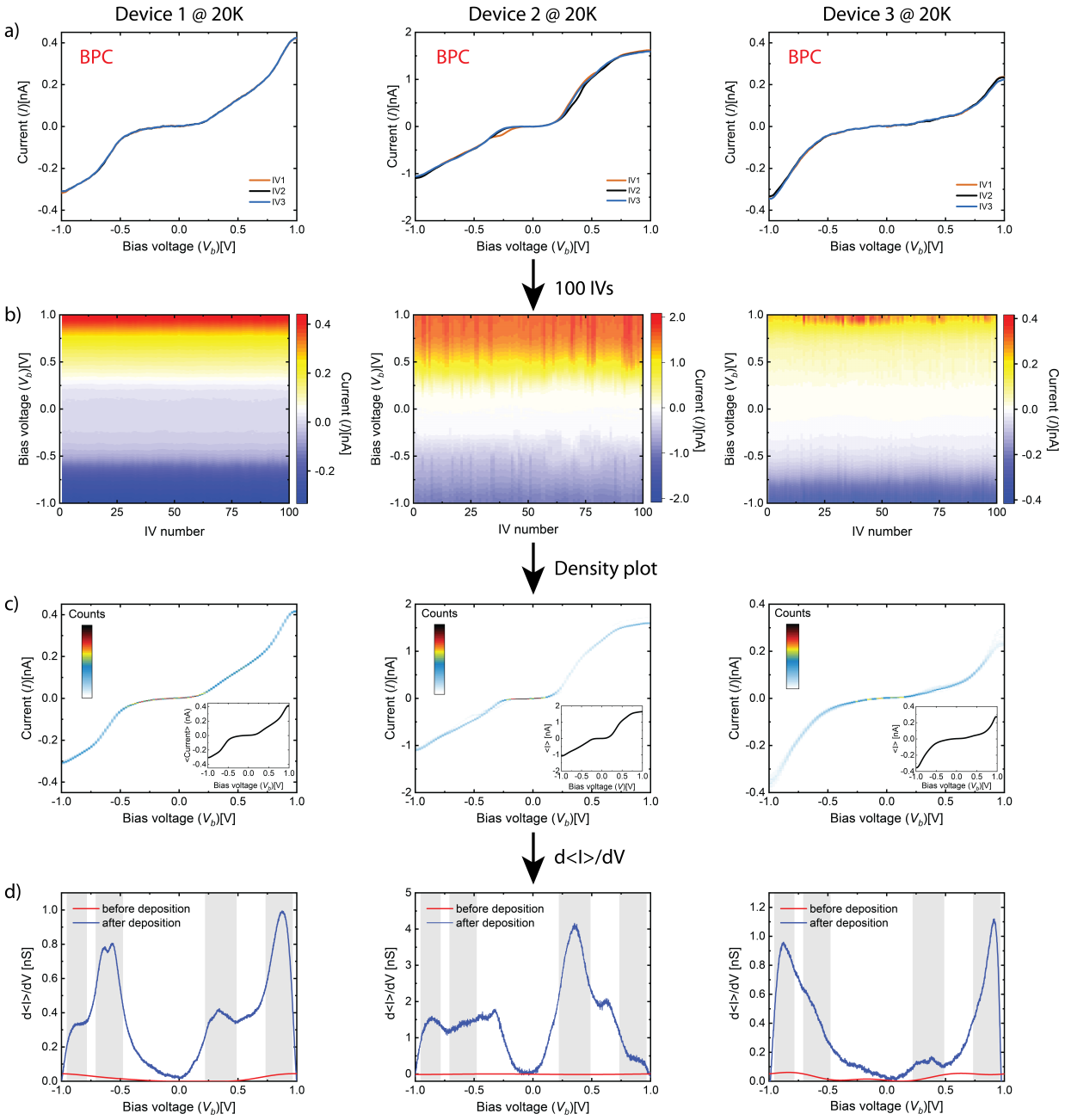

Figure 2: **Characterization of device 1-3 at 20 K exposed to molecule BPC.** a) Three individual IVs recorded for each device. b) Evolution plot of the current for 100 successive IV-curves. c) Density plots of IVs. The inset shows the average IV curve $\langle I \rangle$. d) d$\langle I \rangle$/dV curve obtained before (red) and after (blue) deposition. The resonances observed after deposition correspond to electronic energy levels of the molecular junction. The grey regions highlight the different resonances.

stable, even though the electronic transport is not. In the Supporting Information, using a statistical cross-correlation analysis, we show that similar electronic features are observed

across multiple devices, demonstrating that indeed the anchoring to the substrate provides sufficient mechanical stability. However, due to the smaller π-π overlap between the head groups compared to the BPC molecule, the electronic stability is limited.

Electronic robustness of the junctions at different temperatures

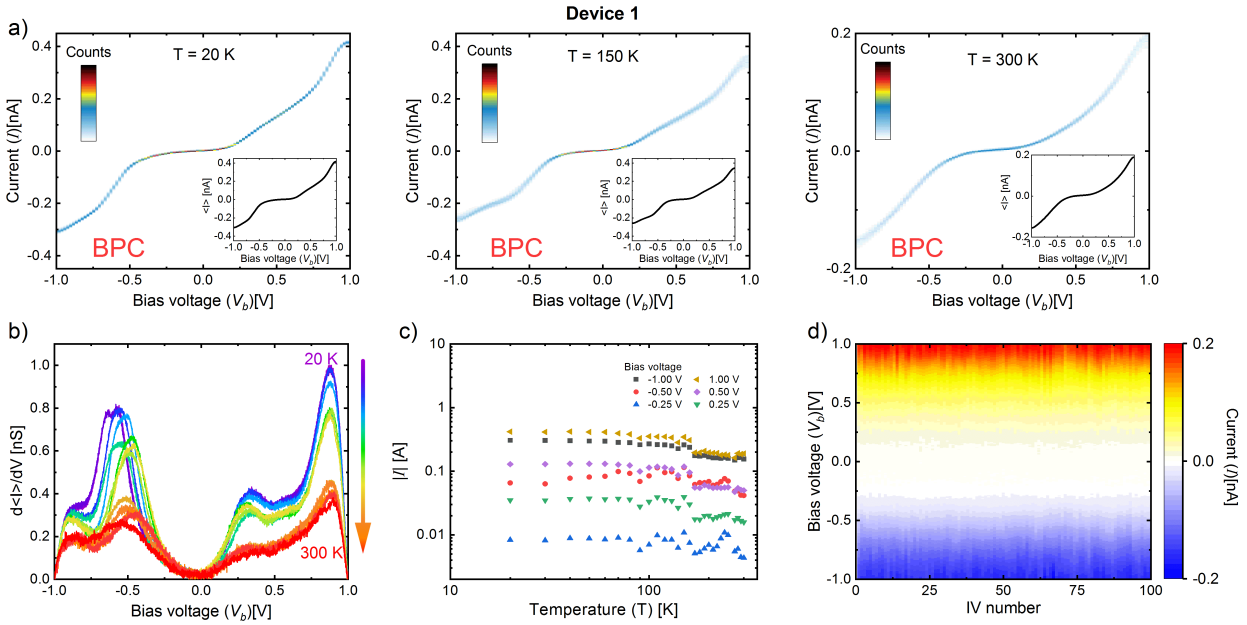

Figure 3: **Transport measurements through a BPC molecular junction (device 1) at different temperatures.** a) Density plots constructed from 100 IVs for the three temperatures. b) Differential conductance $d\langle I\rangle/dV$ of the device shown in a) plotted for increasing temperatures. c)Evolution of the absolute value of $\langle I\rangle$ as a function of the temperature plotted for different bias values in log-log scale. d) Evolution over time of the IV curves measured at 300 K.

To further investigate the junction stability, the devices were characterized in a large range of temperature extending from 20 K to room temperature. Figure 3a shows the density plot obtained from 100 IV curves measured at three selected temperatures (20 K, 150 K and 300K) for device 1, with $\langle I\rangle$ as inset. From the density plots, the high similarity between successive IV curves is observed at all temperatures. This behaviour highlights the

high electronic and mechanical stability of the devices, in stark contrast to the behaviour of junctions based on molecule C (Fig. 1d). A similar observation can also made in Fig. 3b. Here, the plot shows the evolution of $\mathrm{d}\langle I\rangle/\mathrm{dV}$ with temperature. The resonance positions remain fairly similar throughout the entire range, while the peak amplitude steadily decays with increasing temperature.

For a more in-depth characterization of the effect of temperature, Fig. 3c presents the evolution of $\langle I\rangle$ as a function of temperature, plotted in a logarithmic scale. The plot shows that the current remains fairly constant over the entire temperature range for various bias voltage values, and in particular in the high temperature region between 150 K and 300 K. This observation suggests that charge transport though these graphene-molecule-graphene junctions remains coherent up to 300 K. This appealing effect is in contrast with studies performed in systems in which electrons are transported incoherently through the device. In that case a strong reduction in current is observed for decreasing temperatures, corresponding to activation energies in the 10-100 meV range.[37–42] Interestingly, the current through our device even slightly increases with decreasing temperature. This effect may be related to minor rearrangements of the molecules in the junction, which may also be the cause for the small jump in current measured around 120 K. The temperature dependence of the empty graphene gaps was also investigated (see Supporting Information for more details), but no significant effect of temperature was observed, in agreement with a previous study.[16] Finally, Fig. 3d presents the evolution of the IV curves over time at room temperature. Here, no significant fluctuations were observed at bias values up to 2.0 V, highlighting the very high stability of the molecular junctions.

To investigate charge transport through these graphene/molecule/graphene junctions, we calculated the transmission probability $T(E)$ of electrons with energy E passing through the molecules from one graphene electrode to another. We obtain the material specific mean-field Hamiltonian from the SIESTA implementation of density functional theory[43] combined

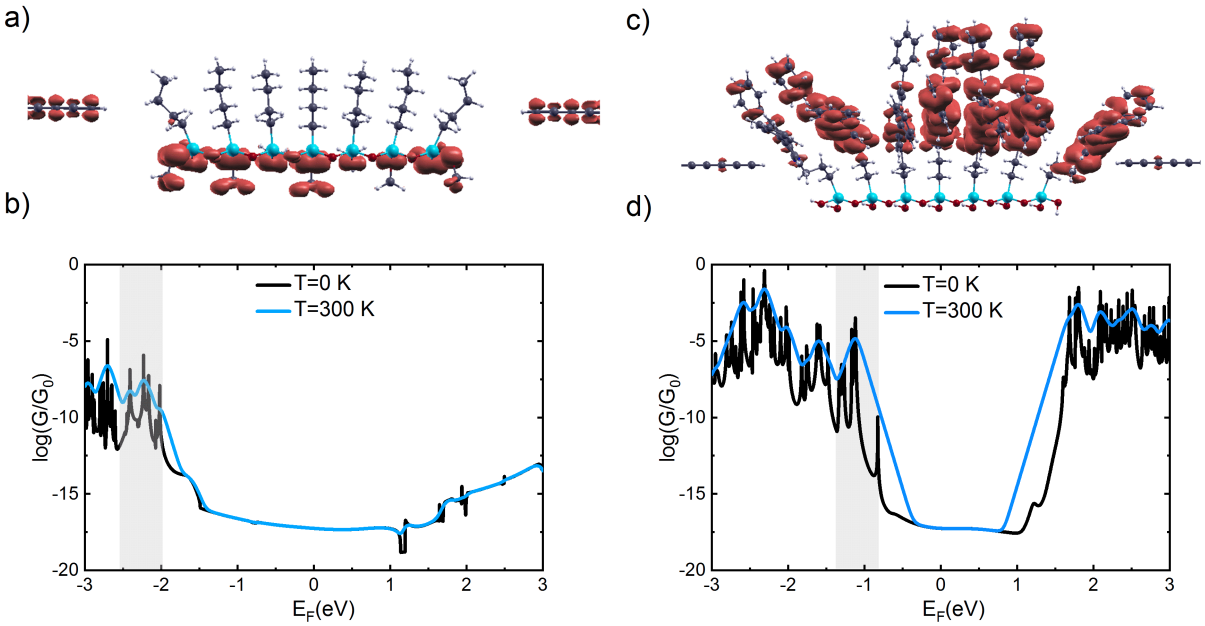

Figure 4: **Transport through graphene/molecule/graphene junctions containing the M and BPC molecule.** (a,b) Computed conductance (G/G_0) of a junction containing molecules M for different Fermi energies (E_F) at $T = 0K$ and room temperature ($T = 300K$) in a junction containing molecules M. Local density of states ($LDOS$) for the shaded region in (b) showing that the wave function does not extended over the alkane groups. (c,d) Computed conductance (G/G_0) of a junction containing molecules BPC for different Fermi energies (E_F) at $T = 0K$ and room temperature ($T = 300K$). Local density of states ($LDOS$) for the shaded region in (d) shows that wave function is extended over the carbazole groups. Note that E_F is the Fermi energy of the junctions relative to the DFT predicted Fermi energy, and may be different from the experiments. The grey-shaded area corresponds to the resonance closest to the Fermi energy of the electrodes.

with the Gollum implementation of the non-equilibrium Green's function method to calculate T(E)[44] (see computational method). The conductance G was calculated for different Fermi energies and temperatures using the Landauer formula: $G = G_0 \int dET(E)(-df/dE)$ where $f = (1 + exp((E - E_F)/K_BT))^{-1}$ is the Fermi Dirac distribution function, T is the temperature, and $k_B = 8.6 \times 10^{-5} eV/K$ is Boltzmann's constant.

Figure 4 shows the computed conductance (G/G_0) for reference molecule M and molecule BPC for a particular junction geometry. Transmissions were also calculated for other geometries (see Supplementary Information). The calculations show that the transmission through the reference molecules is systematically lower than for the BPC molecule, regardless of the

choice of the Fermi energy. This observation also holds for other junction configurations (see Supplementary Information). The drastically lower conductance is attributed to the HOMO-LUMO gap of the graphene/molecule/graphene junction being larger for reference molecule M. To investigate the nature of the transport channels dominating transport for both molecule, Fig. 4a and 4c display the local density-of-states obtained in the energy window highlighted in grey, corresponding to the resonance closest to the Fermi energy. For the BPC molecule, the wave function extends over the biphenyl N-carbazole groups. For the reference molecule, on the other hand, no delocalized orbitals are formed and transport occurs via the poorly conducting silane groups. These calculations demonstrate the crucial role of $\pi - \pi$ stacked head groups in the transport, and rationalize the large difference in current observed experimentally for the two molecules.

Conclusion

This work shows the realization of electronically and mechanically stable graphene based molecular devices over a large range of temperature. This is achieved by decoupling the mechanical anchoring from the electronic pathways by combining a covalent binding of the molecules to the substrate and large π-conjugated head groups. The junctions are reproducible throughout several devices and operate from 20 K up to room temperature. Our approach represents a simple but powerful strategy for the future integration of novel molecule-based functions into stable and controllable nano-electronic devices.

Methods

Molecular synthesis: M and C molecules were purchased from Sigma-Aldrich. Details of the synthesis of the BPC molecule are presented in the supplementary information.

Molecular Dynamic: In order to understand how the 3-carbazolylpropyltrimethoxysilane

molecules are interacting with graphene electrodes, molecular dynamic simulation was carried out using ADF[45] reaxFF package. The Velocity Verlet+Berendsen MD method were used with 0.250 fs time step. The atomic positions belong to the SiO_2 substrate and a part of graphene electrodes far from scattering region were constrained. The simulation run for 150000 MD-iterations. The snapshot of atomic coordinates of the junction were taken. These coordinates were used as initial geometries of the device for the density functional theory calculations.

Density functional theory calculation: The optimized geometry and ground state Hamiltonian and overlap matrix elements of each structure studied in this paper were self-consistently obtained using the SIESTA[43] implementation of the density functional theory (DFT). SIESTA employs norm-conserving pseudo-potentials to account for the core electrons and linear combinations of atomic orbitals (LCAO) to construct the valence states. The generalized gradient approximation (GGA) of the exchange and correlation functional is used with the Perdew-Burke-Ernzerhof (PBE) parameterization and a double-ζ polarized (DZP) basis set. The real-space grid is defined with an equivalent energy cut-off of 250 Ry. The geometry optimization for each structure is performed to the forces smaller than 20 meV/$\mathring{A}$.

Transport: The mean-field Hamiltonian obtained from the converged SIESTA DFT calculation was combined with Gollum[44] implementation of the non-equilibrium Green's function method, to calculate the phase-coherent, elastic scattering properties of the each system consist of left (source) and right (drain) graphene leads connected to the scattering region formed from 3-carbazolylpropyltrimethoxysilane molecules. The transmission coefficient T(E) for electrons of energy E (passing from the source to the drain) is calculated via the relation $T(E) = trace(\Gamma_R(E)G^R(E)\Gamma_L G^{R\dagger}(E))$. In this expression, $\Gamma_{L,R} = i(\Sigma_L, R(E) - \Sigma_L, R^\dagger(E))$ describe the level broadening due to the coupling between left (L) and right (R) electrodes and the central scattering region, are the retarded self-energies associated with this coupling and $G^R = (ES - H - \Sigma_L - \Sigma_R)^{-1}$ is the retarded Green's function, where H is the Hamiltonian and S is the overlap matrix. Using the obtained transmission coefficient, the conductance is calculated by Landauer formula $G = G_0 \int dET(E)(-\partial f(E,T)\partial E)$ where $G_0 = 2e^2/h$ is the conductance quantum, $f(E,T) = (1 + exp((E - E_F)/k_BT)^{-1}$ is the Fermi-Dirac distribution function, T is the temperature and $k_B = 8.6^{-5}$ eV/K is Boltzmann's constant.

Acknowledgments

We would like to thank Christian Schönenberger for fruitful discussions. This work was partially funded by the EC FP7-ITN MOLESCO grant (N° 606728) and the FET open project QuIET (N° 767187). This work was supported by U.K. EPSRC Grant EP/M014452/1 and EP/N017188/1 and the ERC Advanced grant (Mols@Mols). H.S. acknowledge the Leverhulme Trust for Leverhulme Early Career Fellowship N° ECF-2017-186. M.P. acknowledges the funding by the EMPAPOSTDOCS-II programme which has received funding from the European Union's Horizon 2020 research and innovation programme under the Marie Skłodowska-Curie Grant Agreement N° 754364.

Author contributions

M.E conducted the measurements and performed the data analysis. O.B. and M.E. fabricated the devices. X.L, S-X.L., S.D and S.Y provided the molecules. S.S and H.S performed the DFT calculations. M.E., M.P., H.S.J.Z., C.L and M.C. designed and supervised the study. M.E., M.P., S.S. and H.S. wrote the paper. M.E., M.P., S.S., H.S., M.C. participated in the discussion of the data. All authors commented the manuscript.

Competing interests

The authors declare no competing financial interests.

Materials & Correspondence

Correspondence and request of materials regarding theoretical calculations should be addressed to H.S, regarding the synthesis to S-X.L. and those regarding the experiments to M.C.

Data availability

The data that support the plots within this paper and other findings of this study are available from the corresponding authors upon reasonable request.

References

(1) Manzeli, S., Ovchinnikov, D., Pasquier, D., Yazyev, O. V. Kis, 2D transition metal dichalcogenides. *Nat. Rev. Mater.* **2017**, 17033.

(2) Cha, Eunho, Patel, Mumukshu D., Park, Juhong, Hwang, Jeongwoon,Prasad, Vish, Cho, Kyeongjae, Choi, Wonbong, 2D MoS2 as an efficient protective layer for lithium metal anodes in high-performance Li–S batteries. *Nature Nanotechnology* **2018**, 1748–3395.

(3) Anindya Nag,; Arkadeep Mitra,; Subhas Chandra Mukhopadhyay, Graphene and its sensor-based applications: A review. *Sensors and Actuators A: Physical* **2018**, *270*, 177–194.

(4) Rodrigo, D.; Limaj, O.; Janner, D.; Etezadi, D.; Garc\'\ia de Abajo, F. Javier,; Pruneri, V.; Altug, H. Mid-infrared plasmonic biosensing with graphene. *Science* **2015**, *349*, 165–168.

(5) Fu, W.; Feng, L.; Panaitov, G.; Kireev, D.; Mayer, D.; Offenhäusser, A.; Krause, H.-J. Biosensing near the neutrality point of graphene. *Science Advances* **2017**, *3*.

(6) Wang, Qing Hua,Kalantar Zadeh, Kourosh, Kis, Andras,Coleman, Jonathan N., Strano, Michael S., Electronics and optoelectronics of two-dimensional transition metal dichalcogenides. *Nature Nanotechnology* **2012**, *7*, 699.

(7) Radisavljevic, B., Radenovic, A.,Brivio, J.,Giacometti, V.,Kis, A., Single-layer MoS2 transistors. *Nature Nanotechnology* **2012**, *6*, 147.

(8) Koppens, F. H. L., Mueller, T., Avouris, Ph., Ferrari, A. C., Vitiello, M. S., Polini, M., Photodetectors based on graphene, other two-dimensional materials and hybrid systems. *Nature Nanotechnology* **2014**, *9*, 780.

(9) Tuma, Tomas, Pantazi, Angeliki,Le Gallo, Manuel,Sebastian, Abu, Eleftheriou, Evangelos, Stochastic phase-change neurons. *Nature Nanotechnology* **2016**, *11*, 693.

(10) Yang, J. Joshua, Strukov, Dmitri B.,Stewart, Duncan R., Memristive devices for computing. *Nature Nanotechnology* **2012**, *8*, 13.

(11) Prezioso, M.,Merrikh-Bayat, F.,Hoskins, B. D.,Adam, G. C., Likharev, K. K.,Strukov, D. B., Training and operation of an integrated neuromorphic network based on metal-oxide memristors. *Nature* **2015**, *61*, 521.

(12) Sangwan, Vinod K.,Lee, Hong-Sub, Bergeron, Hadallia,Balla, Itamar, Beck, Megan E.,Chen, Kan-Sheng, Hersam, Mark C., Multi-terminal memtransistors from polycrystalline monolayer molybdenum disulfide. *Nature* **2018**, *554*, 500.

(13) Lee, C.; Wei, X.; Kysar, J. W.; Hone, J. Measurement of the Elastic Properties and Intrinsic Strength of Monolayer Graphene. *Science* **2008**, *321*, 385–388.

(14) Falkovsky, L. A. Optical properties of graphene. *Journal of Physics: Conference Series* **2008**, *129*, 012004.

(15) Berger, C.; Song, Z.; Li, X.; Wu, X.; Brown, N.; Naud, C.; Mayou, D.; Li, T.; Hass, J.; Marchenkov, A. N.; Conrad, E. H.; First, P. N.; de Heer, W. A. Electronic Confinement and Coherence in Patterned Epitaxial Graphene. *Science* **2006**, *312*, 1191–1196.

(16) Prins, F.; Barreiro, A.; Ruitenberg, J. W.; Seldenthuis, J. S.; Aliaga-Alcalde, N.; Vandersypen, L. M.; van der Zant, H. S. Room-temperature gating of molecular junctions using few-layer graphene nanogap electrodes. *Nano letters* **2011**, *11*, 4607–4611.

(17) Sadeghi, H.; Mol, J. A.; Lau, C. S.; Briggs, G. A. D.; Warner, J.; Lambert, C. J. Conductance enlargement in picoscale electroburnt graphene nanojunctions. *Proceedings of the National Academy of Sciences* **2015**, *112*, 2658–2663.

(18) Nef, C.; Pósa, L.; Makk, P.; Fu, W.; Halbritter, A.; Schönenberger, C.; Calame, M. High-yield fabrication of nm-size gaps in monolayer CVD graphene. *Nanoscale* **2014**, *6*, 7249–7254.

(19) Jia, C. et al. Covalently bonded single-molecule junctions with stable and reversible photoswitched conductivity. *Science* **2016**, *352*, 1443–1445.

(20) Visions for a molecular future. *Nature Nanotechnology* **2013**, *8*, 385–389.

(21) Aradhya, S. V.; Venkataraman, L. Single-molecule junctions beyond electronic transport. *Nature nanotechnology* **2013**, *8*, 399–410.

(22) Sadeghi, H.; Sangtarash, S.; Lambert, C. Robust Molecular Anchoring to Graphene Electrodes. *Nano Letters* **2017**, *17*, 4611–4618.

(23) Tao, N. Electron transport in molecular junctions. *Nature nanotechnology* **2006**, *1*, 173–181.

(24) Lau, C. S.; Sadeghi, H.; Rogers, G.; Sangtarash, S.; Dallas, P.; Porfyrakis, K.; Warner, J.; Lambert, C. J.; Briggs, G. A. D.; Mol, J. A. Redox-dependent Franck–Condon blockade and Avalanche transport in a graphene–fullerene single-molecule transistor. *Nano letters* **2015**, *16*, 170–176.

(25) Barreiro, A.; van der Zant, H. S.; Vandersypen, L. M. Quantum dots at room temperature carved out from few-layer graphene. *Nano letters* **2012**, *12*, 6096–6100.

(26) Gehring, P.; Sadeghi, H.; Sangtarash, S.; Lau, C. S.; Liu, J.; Ardavan, A.; Warner, J. H.; Lambert, C. J.; Briggs, G. A. D.; Mol, J. A. Quantum interference in graphene nanoconstrictions. *Nano letters* **2016**, *16*, 4210–4216.

(27) Su, T. A.; Neupane, M.; Steigerwald, M. L.; Venkataraman, L.; Nuckolls, C. Chemical principles of single-molecule electronics. *Nature Reviews Materials* **2016**, *1*, 16002.

(28) Li, S.; Li, Q.; Carpick, R. W.; Gumbsch, P.; Liu, X. Z.; Ding, X.; Sun, J.; Li, J. The evolving quality of frictional contact with graphene. *Nature* **2016**, *539*, 541–545.

(29) Mol, J. A.; Lau, C. S.; Lewis, W. J.; Sadeghi, H.; Roche, C.; Cnossen, A.; Warner, J. H.; Lambert, C. J.; Anderson, H. L.; Briggs, G. A. D. Graphene-porphyrin single-molecule transistors. *Nanoscale* **2015**, *7*, 13181–13185.

(30) Xu, Q.; Scuri, G.; Mathewson, C.; Kim, P.; Nuckolls, C.; Bouilly, D. Single Electron Transistor with Single Aromatic Ring Molecule Covalently Connected to Graphene Nanogaps. *Nano letters* **2017**, *17*, 5335–5341.

(31) Yao, J.; Zhong, L.; Natelson, D.; Tour, J. M. Silicon Oxide: A Non-innocent Surface for Molecular Electronics and Nanoelectronics Studies. *Journal of the American Chemical Society* **2011**, *133*, 941–948.

(32) Pósa, L.; El Abbassi, M.; Makk, P.; Sánta, B.; Nef, C.; Csontos, M.; Calame, M.; Halbritter, A. Multiple Physical Time Scales and Dead Time Rule in Few-Nanometers Sized Graphene–SiO x-Graphene Memristors. *Nano letters* **2017**, *17*, 6783–6789.

(33) El Abbassi, M.; Pósa, L.; Makk, P.; Nef, C.; Thodkar, K.; Halbritter, A.; Calame, M. From electroburning to sublimation: substrate and environmental effects in the electrical breakdown process of monolayer graphene. *Nanoscale* **2017**, *9*, 17312–17317.

(34) Aswal, D.; Lenfant, S.; Guerin, D.; Yakhmi, J.; Vuillaume, D. Self assembled monolayers on silicon for molecular electronics. *Analytica Chemica Acta* **2006**, *568*, 84–108.

(35) DiBenedetto, S. A.; Facchetti, A.; Ratner, M. A.; Marks, T. J. Molecular Self-Assembled Monolayers and Multilayers for Organic and Unconventional Inorganic Thin-Film Transistor Applications. *Advanced Materials* **2009**, *21*, 1407–1433.

(36) Krasnoslobodtsev, A. V.; Smirnov, S. N. Effect of Water on Silanization of Silica by Trimethoxysilanes. *Langmuir* **2002**, *18*, 3181–3184.

(37) Hines, T.; Diez-Perez, I.; Hihath, J.; Liu, H.; Wang, Z.-S.; Zhao, J.; Zhou, G.; Mullen, K.; Tao, N. Transition from tunneling to hopping in single molecular junctions by measuring length and temperature dependence. *Journal of the American Chemical Society* **2010**, *132*, 11658–11664.

(38) Segal, D.; Nitzan, A.; Davis, W. B.; Wasielewski, M. R.; Ratner, M. A. Electron transfer rates in bridged molecular systems 2. A steady-state analysis of coherent tunneling and thermal transitions. *The Journal of Physical Chemistry B* **2000**, *104*, 3817–3829.

(39) Kim, H.; Segal, D. Controlling charge transport mechanisms in molecular junctions: Distilling thermally induced hopping from coherent-resonant conduction. *The Journal of chemical physics* **2017**, *146*, 164702.

(40) Hihath, J. Charge transport in the inverted Marcus region. *Nature nanotechnology* **2018**, 1.

(41) Yuan, L.; Wang, L.; Garrigues, A. R.; Jiang, L.; Annadata, H. V.; Antonana, M. A.; Barco, E.; Nijhuis, C. A. Transition from direct to inverted charge transport Marcus regions in molecular junctions via molecular orbital gating. *Nature nanotechnology* **2018**, 1.

(42) Selzer, Y.; Cabassi, M. A.; Mayer, T. S.; Allara, D. L. Thermally activated conduction in molecular junctions. *Journal of the American Chemical Society* **2004**, *126*, 4052–4053.

(43) Soler, J. M.; Artacho, E.; Gale, J. D.; García, A.; Junquera, J.; Ordejón, P.; Sánchez-Portal, D. The SIESTA method for ab initio order-N materials simulation. *Journal of Physics: Condensed Matter* **2002**, *14*, 2745.

(44) Ferrer, J.; Lambert, C. J.; García-Suárez, V. M.; Manrique, D. Z.; Visontai, D.; Oroszlany, L.; Rodríguez-Ferradás, R.; Grace, I.; Bailey, S.; Gillemot, K.; Sadeghi, H.; Algharagholy, L. GOLLUM: a next-generation simulation tool for electron, thermal and spin transport. *New Journal of Physics* **2014**, *16*, 093029.

(45) K. Chenoweth,; A.C.T. van Duin,; W.A. Goddard, ReaxFF reactive force field for molecular dynamics simulations of hydrocarbon oxidation. *Journal of Physical Chemistry A* **2008**, *112*, 1040–1053.